A compatibility study of protective coatings for temperature sensor integration into sodium-ion battery cells

Journal of Physics: Energy

PAPER

A compatibility study of protective coatings for temperature sensor integration into sodium-ion battery cells

Timothy A Vincent*, Faduma M Maddar, Sheng Chao, Erdogan Guk, Jonathan E H Sansom, Begum Gulsoy, Mark Copley, Ivana Hasa and James Marco

WMG, The University of Warwick, Coventry CV4 7AL, United Kingdom
* Author to whom any correspondence should be addressed.

E-mail: T.A.Vincent@warwick.ac.uk

Keywords: battery cell instrumentation, smart batteries, thermistor temperature sensing, sodium-ion batteries, conformal coatings, chemical compatability

Supplementary material for this article is available online

OPEN ACCESS

RECEIVED
10 October 2023

REVISED
8 December 2023

ACCEPTED FOR PUBLICATION
12 January 2024

PUBLISHED
2 February 2024

Abstract

Instrumented battery cells (i.e. those containing sensors) and smart cells (with integrated control and communication circuitry) are essential for the development of the next-generation battery technologies, such as Sodium-ion Batteries (SIBs). The mapping and monitoring of parameters, for example the quantification of temperature gradients, helps improve cell designs and optimise management systems. Integrated sensors must be protected against the harsh cell electrolytic environment. State-of-the-art coatings include the use of Parylene polymer (our reference case).

We applied three new types of coatings (acrylic, polyurethane and epoxy based) to thermistor arrays mounted on flexible printed circuit board (PCBs). We systematically analyse the coatings: (i) PCB submersion within electrolyte vials (8 weeks); (ii) analysis of sample inserted into coin cell; (iii) analysis of sensor and cell performance data for 1Ah pouch SIBs. Sodium-based liquid electrolyte was selected, consisting of a 1 M solution of sodium hexafluorophosphate ($NaPF_6$) dissolved in a mixture of ethylene carbonate and diethylene carbonate in a ratio of 3:7 (v/v%). Our novel experiments revealed that the epoxy based coated sensors offered reliable temperature measurements; superior performance observed compared to the Parylene sensors (erroneous results from one sample were reported, under 5 d submersed in electrolyte).

Nuclear magnetic resonance (NMR) spectroscopy revealed in the case of most coatings tested, formation of additional species occurred during exposure to the different coatings applied to the PCBs. The epoxy-based coating demonstrated resilience to the electrolytic-environment, as well as minimal effect on cell performance (capacity degradation compared to unmodified-reference, within 2% for the coin cell, and within 3.4% for pouch cell). The unique methodology detailed in this work allows sensor coatings to be trialled in a realistic and repeatable cell environment. This study demonstrated for the first time that this epoxy-based coating enables scalable, affordable, and resilient sensors to be integrated towards next-generation Smart SIBs.

1. Introduction

Large-scale grid energy storage will be essential to de-carbonising electrical grids and reducing reliance on fossil fuels, as current renewable energies (e.g. solar, wind) are inherently intermittent [1]. Among the proposed electrochemical energy storage solutions, lithium-ion batteries (LIBs) play a primary role in the transition to a low carbon economy, especially in the automotive sector. However, as the market rapidly expands, the environmental and social challenges associated with the mass production of LIBs are generating interest in alternative solutions, based on materials that can be sourced in a sustainable and responsible way.

Sodium-ion batteries (SIBs) represent an alternative low cost, sustainable and more environmentally friendly energy storage technology and are well positioned to be the favoured technology for stationary

storage and many volume transportation applications [2, 3]. The processes and techniques evolved during the development of today's LIBs have strongly accelerated the current development of SIBs as demonstrated by the recent success of several companies investing in the technology aiming at accelerating their deployment as part of the vital energy storage backbone of a renewable energy grid [4, 5]. In order to allow monitoring of vital aspects, such as cycle life, and safety, we build upon our cell instrumentation processes and demonstrate their application to post-lithium cell chemistries.

A protective layer must be applied prior to embedding sensors within a cell, protecting both the sensor from damage and the electrolyte from contamination. Electrolyte is inherently corrosive, thereby embedding an unprotected sensor will cause (1) damage to the sensor (corrosion and ultimate failure of electronic components) and (2) degradation of the cell performance (contaminants from the sensor materials pollute the electrolyte). Prior work in the area of instrumented LIBs [6, 7] has demonstrated the importance of embedding sensing, towards understanding cell operation *in-situ*.

For the first time, we demonstrate the compatibility of sensor coating materials with SIB chemistries, underpinning the methodology of embedding sensors within cells without degrading electrochemical performance. We follow a comprehensive testing routine, involving analysis of electrolyte pre- and post-sensor insertion, to identify a suitable protective coating to allow flexible PCB sensors to be embedded within pouch cells, with negligible impact on cell performance.

In this work, our test procedure includes submersion in an electrolytic environment for a period of 8 weeks. Within the context of this first study, this time was deemed appropriate to ascertain initial proof-of-concept and to underpin future longer-term material compatibility studies. Previous instrumentation studies protect sensors with small scale and expensive coating methods, and typically only test the instrumented cells for a short period (10 s of cycles) [8]. Prior work in the literature is introduced in the Background section below, with further details of our experimental setup discussed in the Methodology.

In this article, to the authors' knowledge, for the first time we perform an in-depth investigation of the compatibility of sensor coating materials for the application of SIBs; we apply particular focus on materials that are affordable, scalable, and can be applied via time-efficient methods. In this preliminary study, to remove experimental variables, the sensors were tested in vials of cell electrolyte, avoiding the need to install the sensors directly into live cells. Sensors protected with tubing serves as a benchmark.

This paper is structured as follows: background–introduction to prior research in the area, and definition of our contribution beyond the current state-of-art cell instrumentation; methodology–description of our experimental setup, and scenarios/sensor materials under test; results and discussion–presentation of our findings and explanation of the experimental data; finally in the Further work and conclusions sections we detail our ongoing work and possible improvements for our future studies, and then briefly summarise our study and key outcomes.

2. Background

The need to obtain precise internal cell measurements of parameters influencing cell performance has driven our study to optimise sensor placement within the cell core. With the demand for higher energy density battery packs, faster charging capabilities, and higher safety content, the development of improved cells (for example, chemistry optimisation, temperature management system refinements and safety improvements), is a field of great interest for both academic and commercial research [9].

Cell Instrumentation (i.e. sensors installed within/around cells) is a key step towards the development of smart cells which help underpin a comprehensive understanding of thermal management requirements. We have demonstrated internal cell monitoring is vital to understand the conditions experienced within the core of a cell; in prior reports with 21700 format cylindrical LIBs, the core temperature was found to be approximately 3 °C hotter, when the cells were tested with a 2 C discharge rate and varied considerably along the length of the cell–where the sensors were protected with heat-shrink tubing [7].

The tube protection method entails strict limits on PCB design, as sensors and circuitry must fit within the tube area (perhaps a 1 mm^2 tube opening). The tube itself adds bulk to the sensor system (shrunk diameter has wall thickness of ∼0.5 mm), preventing 'prongs' or 'fingers' and larger map areas are not possible. The relatively thick width of the tube restricts insertion routes and the application to larger cell formats (M2.5 hole) and prevents placement of the sensor in between layers of the cell structure. Notably, it prohibits pouch cell deployment where the thickness of the assembly would cause non-uniform ridges on the cell surface.

Internal cell monitoring has been noted to offer valuable insights into battery performance [10], regardless of chemistry type, and in particular this information can help guide cell development. In terms of temperature monitoring, and safety evaluation with our developed instrumentation process, internal sensors provide a reliable and repeatable monitoring placement. In terms of monitoring core cell temperature, the

thermistor arrays covering approach offers excellent chemical and physical protection, demonstrated by a prior study conducted over 100 cycles of cylindrical cell ageing [6]. Cylindrical cells, due to their mechanical stability and robustness to internal pressure, are popular with electric vehicle (EV) manufacturers [11].

Pouch cells offer greater flexibility in terms of sizing (thus improving packing efficiency), and are also promising with original equipment manufacturers [11, 12]. In terms of cell development, pouch cells offer an important step between coin and larger format cells [13]. Cell instrumentation is well aligned with this area of research, offering a vital tool to better understand cell performance; in this way, it is imperative the sensor itself does not impact cell performance and can be used with a wide variety of cell/chemical designs.

Our research focus is towards instrumentation solutions that are affordable, scalable, reliable and efficient, moving towards an instrumentation platform, that can be used to benchmark cells' performance. In the following section we discuss the current state-of-art research and our initial work verifying our solutions can be transferred and used comparatively with both LIB and SIB cells.

2.1. SIB technology

LIBs dominate the commercial manufacturing output for EVs and portable electronics with grid storage application rapidly expanding [14, 15]. Achievable LIB specific energy levels, i.e. 180–220 Wh kg^{-1}, cement their place as the current choice for EVs (compared to SIBs of ∼120 and 160 Wh kg^{-1}) [16, 17]. In applications where for a given desired specific energy, the weight, volume and production-costs are constrained (i.e. transportation, portable devices, low-cost scalable manufacturing), LIBs are currently the preferred option [18].

The LIB supply chain is governed by the availability of critical raw materials such as Lithium and Cobalt [19], directly impacting cell cost; reducing reliance on these is acknowledged [20], if not at least due to their finite total availability. Conversely, the abundancy and homogeneous distribution of the raw critical materials used in SIBs strengthens interest in these alternative battery chemistries [21], along with the prospect of reducing the environmental and ethical issues associated with the mining of LIB components.

We aim to demonstrate our instrumentation techniques can be utilised irrespective of cell chemistry, starting here with sodium-ion. The interactions between the electrolyte and sensor must be investigated, to ensure the specific chemistry and sensor coating are compatible. However, the chemical construction of both LIB and SIB electrolytes, in general, entails reasonable similarity, meaning a material found to be suitable for one type will have good potential for use with the other chemistry. In brief, we define a successful pairing if the capacity of the cell is unaffected, and if the sensor demonstrates stable performance.

At least two use cases for instrumented cells are proposed, firstly cell development (optimising cell performance and battery systems etc.), and secondly *in-situ* or in-application deployment. Sensors embedded in the cells during operation would help optimise the performance of the system continuously throughout its life. At end-of-life, the sensors could help triage or grade cells, to immediately indicate which cells are suitable for second-life [22].

2.2. Cell instrumentation

Temperature monitoring is a critical tool to monitor the state of health of battery cells during operation, providing a direct measure of cell performance. The benefits of instrumentation have been in the literature (e.g. thermistor instrumentation [6, 7], thermocouple instrumentation [23]).

During the life of the pack in-application, the battery management system (BMS) usually controls the pack (i.e. thermal management system operation, and charging/discharging rate) using a limited dataset [24]. Due to limited sensor inputs contributing to models, the BMS can only approximate State of Charge (SoC) and pack performance; these approximations are likely to worsen as the pack ages (observations made at a smaller, e.g. individual cell level, do not always scale when used at a system level) [25].

In this work, we selected thermistors to demonstrate the effectiveness of the trial coatings. These sensors offer a cost-effective method for distributed sensing. Multiple devices can be placed on a single substrate, aiding positioning, with all sensors connected via a common ground, minimising wiring. Their effective higher voltage output, i.e. measurement voltage is in range of approximately 0.5–3 V (compared to range of few mV for thermocouples), reduces the reliance on cabling.

2.3. Protective coatings

Prior studies have detailed the use of heat-shrinkable tubing to cover thermistor arrays within 21700 format cylindrical cells [7]. This tubing was demonstrated as forming a chemically resilient barrier, against the harsh electrolytic environment within the LIBs, as well as mechanical support during the instrumentation process, and allowed precise internal temperature measurements. The layer was chemically inert (>100 cycles tested [6]), and also provided physical protection during sensor installation. This method was suited for small laboratory scale production but cannot be scaled to greater production volumes. Similarly, the methods

Table 1. Prior works reporting method of protecting sensors for instrumentation within LIBs.

Experiment aim	Coating material	Summary and comments	References
Measurement of thermal conductivity through plane direction in a cylindrical cell.	Parylene (10 μm thick, applied using special evaporator).	Reliable measurements using miniature thermocouples, tested up to 3 C charge in an 18 650 format cell.	Zhang *et al* [26]
Temperature map of A7 pouch cell.	Parylene (1 μm thick conformal coating).	Thermistor PCB array provided reliable and stable readings, cycled up to C/2.5.	Amietszajew *et al* [27]
Distributed temperature monitoring in A5 pouch cell.	PTFE tube (provides protection and reduces impact of strain on temperature measurements).	Optic fibre sensor provided distributed measurements, cycled up to 5 C discharge.	Yu *et al* [28]
Internal temperature measurement of pouch cell.	Silica covered fibre optic sensors.	Fibres placed in electrolyte for 2 weeks prior to measurements–noted no reaction to electrolyte. Sensor able to measure internal temperature during 8 C cycling.	Novais *et al* [29]
External temperature and strain pouch cell measurements.	Acrylate covered fibre optic sensor.	External measurements only–covering cannot within stand temperatures above 150 °C.	Meyer *et al* [30]
Measurement of the lithiation voltage of graphite within the cell.	Polymer sealing layer (limited details provided).	Embedded fibre optic sensor, tested up to C/6 charge rate.	Ghannoum *et al* [31]
Internal temperature measurement in pouch cell.	Polyimide foil (50 μm thick)–noted as nonconductive, and no reaction to electrolyte.	Fibre optic sensor, covered with the foil. Cell charged up to 4 C rate. Sensor noted to provide reliable and stable readings.	Li *et al* [32]
Internal temperature, voltage and current measurement of coin cell.	Polyimide film protective layer.	Film used to insulate and protect sensor. Tested up to 10 C rate cycle.	Lee *et al* [33]
Internal temperature measurement of pouch cell.	Polyimide film (10 μm thick)–provides flexible substrate and cover layer.	Flexible resistance temperature detector (RTD) developed, tested up to 2 C rate. Good electrical insulation and chemical/temperature stability. Sensor had no effect on cell performance after test of 100 cycles.	Zhu *et al* [34]
Distributed internal temperature measurement of cylindrical cells.	Heat shrinkable tubing (overall approx. 1.8 mm diameter).	Array of thermistor sensors inserted into core of 21700 format cell. No detrimental effect on performance after 100 cycles compared to pristine.	Vincent *et al* [6, 7]
Target for this work–protection for miniature sensors, applicable to range of cell formats.	Polymer based paste, affordable and fit for scalable deployment. Thin coating layer.	Coating potentially suitable for range of sensor types (initial trials with thermistor array). Target no detrimental effect on sensors nor electrolyte for period of at least 8 weeks.	This work.

reported in the literature regarding sensor protection for cell instrumentation, table 1, are based on prototyping sensors, and not verifying coating performance for extended operation and manufacturing scalability.

Parylene coated sensors have been previously described in instrumentation development studies [35]. This coating process is costly, time consuming and complex [36]. It is often noted in the literature as

providing excellent chemical resilience [37], however in terms of scaling, its limitations lead to the eventual selection of an alternative protection method [36]. Stephenson *et al*, note the cost of protecting an electrode array (for biomedical applications) was reduced from ∼$100 to $0.07 per board when changing from using Parylene *C* to polyimide tape [36]. In one initial chemical compatibility trial, it was noted Parylene provided excellent sensor protection, but debris was observed after testing in electrolyte, indicating the possible deterioration of the coating [6].

In the Methodology below, we detail our study expanding the prior art reported in the literature, for example [6]. Here we study sensor performance over a longer period, testing 3 brush-on conformal coatings (readily available off-the-shelf), and report on our comprehensive post-experimentation analysis.

3. Method

Conformal coatings were selected given the following criteria, briefly: (a) scalability, (b) affordability, (c) resilience to harsh chemicals and (d) inertness to cell chemistry. In this work, recyclability of the sensor components was not a primary selection factor, although we note our goal to create an automated and efficient instrumentation process, inherently leads to reduced material usage. Points (a) and (b) were, although qualitative assessments, raised following the obstacles observed with expanding the application of specialist coatings to larger batches, where the process becomes extremely costly, and the application methodology could not be scaled up to fit within a production process. In this proof-of-concept study, the search for candidate coatings was restricted to off-the-shelf products, which were affordable, readily available and did not require specialised equipment to apply.

At this relatively small-scale experimental stage, cost savings possible with high volume procurement cannot be achieved. However, we focus on reducing need for specialist products or processing stages, to reduce labour required during production, which are key to reducing overall cost. In a similar manner, storage in a non-controlled environment and long term (period of weeks) were also desirable to ease processing considerations. These first criteria were achieved via literature review in the area, and manufacturer provided product information. To allow a minimum of 3 repetitions per coating, 3 additional coatings were selected to be trialled alongside the reference protection materials.

3.1. Coating selection and assembly

There is limited information in the literature regarding compatibility with conformal coatings and cell electrolyte. Therefore, to provide reasonable experimentation with a range of material types, 3 distinct types of polymeric coating were selected, namely acrylic, polyurethane and epoxy based. Acrylic was selected as a common material used in cell test rig designs [38], and in sheet format has not been noted to react with electrolyte. Polyurethane is a popular choice as an electrically insulating material [39], and is known to provide a mechanically durable finish. Epoxy has previously been used to adhere materials together during instrumented cell construction [28].

Criteria (c) and (d) cover the experimentation in this study; verifying both the coating was able to protect the sensors itself from damage due to the corrosive nature of electrolyte and the cell chemistry was not contaminated due to the presence of the coated sensor. Table 2 summarises the list of coating types studied. For the small PCBs tested here (<2 mm width, ∼80 mm length), it was estimated <1 ml volume was needed per array; in the case of the protective tubing, ∼70 mm was used per array.

To repeatably reproduce the harsh chemical environment within the cells, containers of electrolyte were prepared to submerge the sensor PCBs. This decouples the sealing and mechanical damage possible by instrumenting a live cell. Glass vials with screw lids were selected, where the lids could be instrumented in the same manner as the proven techniques used with cylindrical cells [7].

Three repetitions were performed per coating (each PCB tested in a separately). This allowed the potential contamination of each coating to be assessed individually, as well as ensuring lower quantities of electrolyte were stored in separate containers. i.e. if a leak were to occur, the volume of electrolyte exposed to the environment would be limited. The sensors under test were identical to those used in 21700 LIB cylindrical cells [7], designed to provide distributed measurements within the cell. Due to the reduced height of the vial, compared to a typical 21700 cell, only the final two sensor positions were submerged in the electrolyte. This however was sufficient to provide two measurement points, and to ensure the coating was spread uniformly across the PCB, albeit an approximate ∼20 mm length of the PCB was under observation.

To verify adequate and uniform coating coverage, the PCBs were inspected under a microscope with UV light after the coatings had been brushed-on (application method described in Supplementary Material). Example images of the PCBs during and immediately after the coating process are shown in figure S2, where the epoxy coating type (iii) was applied.

Table 2. List of protective coatings trialled in this work. Costings here are based on the cost of the coating procured and estimated number of PCBs protected with the supplied volume.

No.	Coating Type	Approx. cost. (quantity supplied) {∼ cost per cell}	Notes
(i)	Acrylic based	∼$20 (500 ml) {∼$0.04}	Conformal coating–protection in high humidity environments. Supplied in a can.
(ii)	Polyurethane based	∼$10 (250 ml) {∼$0.04}	Conformal coating–protection against chemicals, dust, moisture and extreme temperatures. Supplied in a can.
(iii)	Epoxy based	∼$100 (1350 ml) {∼$0.07}	Conformal coating–protection against chemicals, humidity, corrosion, thermal shock and abrasion. Two parts, supplied in cans–mix at time of application.
(iv)	Polyolefin heat-shrink tube	∼$20 (1.2 m) {∼$1.33}	Covering is shrunk over the sensors–protection against chemicals and humidity. Supplied in lengths. Reference case, demonstrated in previous work [6, 7].
(v)	Parylene	∼$30 (per board)	Specialist coating for protection against chemicals. Previously reported in literature, and used in [35].

Table 3. Summary of devices under test.

Vial no.	Coating type	Notes
(1–3)	(iii) Epoxy based	2x sensors per PCB.
(4–6)	(ii) Polyurethane based	2x sensors per PCB.
(7–9)	(i) Acrylic based.	2x sensors per PCB, except damage during assembly to PCB in vial 7.
(10–12)	(iv) Polyolefin tube.	2x sensors per PCB.
(13–15)	None.	2x sensors per PCB. Bare PCB with no coating applied.
(16, 17)	(v) Parylene.	Sensors all populated, but 2x submerged. 100 kΩ thermistors. Note only two sets under test.
(18, 19)	Reference Thermocouple.	Constructed in-house, *K* Type.

The brush-on technique was found to provide good coverage, although a smoother finish could have been achieved via spraying [40]. The slight imperfections in the surface were deemed negligible to performance–in this batch, a total of five PCBs were coated for each coating type, with the three with the best observable finish selected for experimentation. The tracer element helped identify PCBs with poor coverage (which were either discarded or re-coated); however, as visible in figures S2(b)–(e), the relatively small/narrow PCB (1.8 mm width) and thin coating layer limited the observability of the tracer.

The flexible PCBs are received bare from manufacture, with no components populated. Prior to the coating process, the thermistor sensors are soldered onto the substrates–here the lower two sensor positions only are completed (the 2 which will be submerged in the vial). Thermistors with a nominal 10 kΩ resistance at 25 C were selected (Murata NCP03XH103F05RL [41]) for compatibility with the bench top measurement system. The Parylene coated PCBs were assembled and coated by a specialist supplier; these were designed with 100 kΩ nominal resistance thermistors (Murata NCP03WF104F05RL [41]).

In final applications, typical film thicknesses would be in the order of $<100\ \mu$m. However, due to the manual application brush-on technique, coated layers here were noted to be $\sim 150\ \mu$m thick. Comprehensive coverage (particularly the steps from thermistor surface to substrate) was prioritised, to ensure an accurate assessment of the chemical resistance of the coatings without uncertainty of the adeptness of the manual coating process. In this case, the thickness of the coating may affect sensor response, although the focus here is the longevity of both the electrochemistry and the sensor (i.e. sensor response time etc. will not be investigated). It is proposed the tracer would provide better indication when used with physically larger PCBs, or when there is a risk of taller components creating a shadow (missing coating). The complete list of tested devices is shown in table 3.

3.2. Electrolyte submersion

The PCBs were submerged in a commercially available electrolyte, composed of $NaPF_6$ (sodium hexafluorophosphate) salt dissolved in a mixture of solvents including ethylene carbonate (EC) and diethylene carbonate (DEC) in a ratio of 3:7 (v/v %). This electrolyte was suitable for the development of SIBs as well as being representative (in terms of chemical compatibility) to demonstrate the performance of the coatings and provide an indicative result for other electrolytes for LIBs and SIBs.

Post-coating, the sensor PCBs were prepared for instrumentation. The procedure of installing a brass fitting on the PCB array has been discussed in previous work [7]. Briefly, the PCB is threaded through the

centre of the fitting and adhesive heat-shrink used to seal between the fitting and the PCB substrate. In this case, the PCB is positioned with the end ∼20 mm remaining to be inserted into the vial (our standard procedure would be ∼65 mm for a 21700-format cell). This length permits the end 2 sensors to be submerged, without the end of the PCB interfering with the bottom of the vial. To prepare the vials for sensor insertion, the lids are drilled in a similar manner to that used to instrument cylindrical cells. The sensors can be prepared and installed in the lids of the vials outside of a glovebox.

The electrolyte filling is performed within a glovebox (argon environment, water and oxygen levels <0.5 ppm). The components were placed in a drying oven at 60 °C for a period of 24 h, prior to the filling. The vials were filled with ∼1.5 ml of electrolyte using a syringe, in all cases ensuring sufficient quantity was dispensed to cover the two sensors. The lid of the vial was sealed and wrapped with parafilm. This additional seal was implemented to prevent moisture ingress, as the electrolyte is stored outside an inert environment for a prolonged period (8 weeks).

3.3. Experimental setup

The vials were well suited for placement in a block heater (Techne Dri-Block Digital Heater DB100/2TC), to maintain a constant temperature. In effect, the selected heater was designed to house 2 ready-made aluminium blocks, each with 20 slots to hold 12 mm diameter vials and maintain a constant temperature. In this work, a temperature of 25 °C was selected (using one block, to contain up to 20 vials), although it is proposed higher temperatures could be trialled to represent the cell heating during operation.

The heater block assembly along with the data logging equipment, was placed in a fume extraction hood. This ensured the experiment was continuously ventilated, mitigating the potential risk of Hydrogen Fluoride (HF) exposure, if the seal of any vial was to fail. However, this limited the control of the environmental temperature (typically experiments with live cells are performed in climate chambers [7]).

To monitor the sensor performance, criteria (c), thermistor sensor resistance data were logged using a bench-top meter (Keithley DAQ6510) at a rate of 1 measurement every 2 mins (16-bit resolution). The meter was equipped with a multiplexed data acquisition (DAQ) card (Keithley 7708), enabling up to 20 sensors to be logged per card slot (differential measurements). Adaptors were built to connect the flexible electrical connectors on the sensor PCBs to the wires needed to screw-in to the terminals on the DAQ card. Manufacturer software (Keithley Kickstart 2.4.0) was used to configure the sensor type, and log the data. Custom thermocouples, designed for cell instrumentation [23], were used as reference sensors and were assembled for this work. The meter recorded thermistor sensor data in terms of resistance (the functionality to directly record temperature was not utilised here); thermocouple sensor data were recorded in terms of temperature (°C). Thermistor resistance data (R_{Therm}) were converted to temperature readings, via (1) based the manufacturer's datasheet [41]. The constant β equalled 3434 and 4311, for the 10 kΩ and 100 kΩ nominal (R_{Nom}) sensors, respectively. All post-processing was performed via Mathworks MATLAB 2022b. The experimental setup is shown in figure 1, during the initial phase of the test period.

$$\text{Temperature } ^{\circ}\text{C} = \frac{1}{\frac{1}{298.15} - \frac{\ln(R_{\mathrm{Nom}}/R_{\mathrm{Therm}})}{\beta}} - 273.15 \tag{1}$$

After the experimental period was completed, data logging was stopped, and the vials were returned to a glovebox environment for analysis. Assessment of the electrolyte condition was also performed, i.e. to ensure the coated sensors could be used in a cell without contamination or detrimental effect on cell operation, criteria (d).

This assessment comprised two phases, firstly visual inspection of the vial to observe if any debris or discolouration occurred. Secondly, nuclear magnetic resonance (NMR) spectroscopy of the electrolyte liquid recovered after the exposure test, to detect potential decomposition products formed as a result of the reactivity between the coated PCBs and the liquid electrolyte. It is noted, any degradation of the coating (i.e. debris in the vial, or additional compounds identified via NMR) will thereby result in the coating being categorised as providing insufficient protection. Here, the complete submersion of the sensor provides a worst-case scenario in terms of exposing the coating to harsh conditions, however, as cell lifetimes need to be in the order of years, any performance degradation during these accelerated tests will still indicate eventual failure if deployed in a cell.

To practically demonstrate if the sensors disrupted battery performance, beyond analytical methods, small samples of the flexible sensor arrays were placed inside coin cells, as shown in figure 2(a). A small section of PCB (containing 1 sensor) was used in the coin cell–and was located in the middle of the stack (on top of the separator, facing the cathode). The capacity of these cells was measured during cycling, and compared to reference cells, i.e. cells with no sensor element, to verify any detrimental behaviour.

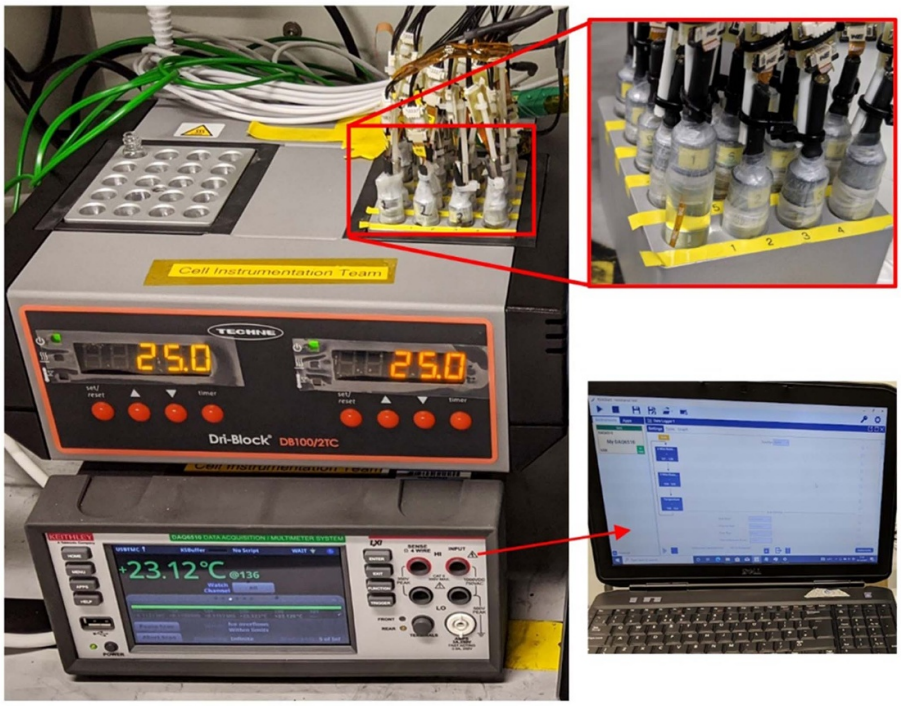

Figure 1. Photograph of experimental setup and data logging apparatus (block heater top, DAQ unit bottom). Inset image shows vials filled with electrolyte and sealed.

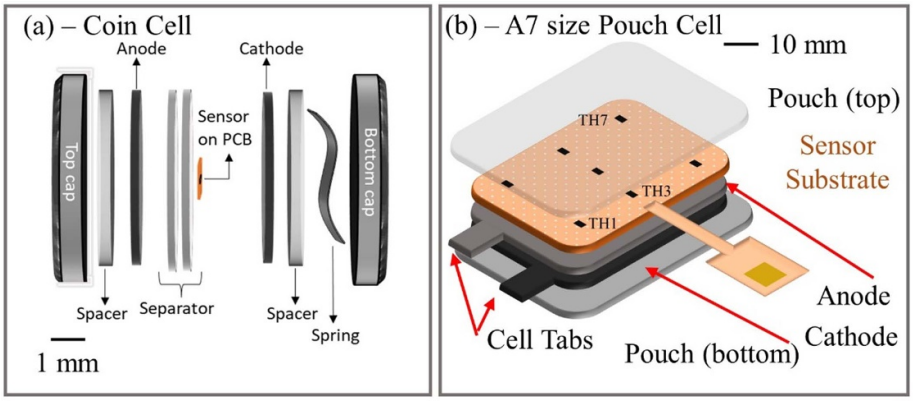

Figure 2. Diagrams showing assembly of instrumented cells with coated sensors (a) coin cell assembly (sample of sensor array placed on the separator layer in the centre of cell, facing cathode) and (b) A7 size pouch cell assembly (sensor array located on top of cell stack, affixed to the top layer of the separator, facing the anode).

This was then expanded to instrumentation of a 1 Ah SIB (pouch format, A7 size, 70 × 100 mm), shown in figure 2(b). The 7-thermistor sensor array substrate (polyimide) was affixed to the top of the cell stack (placed internally on top of the separator facing the anode), shown in the diagram. An identical reference array was also located on the surface of the cell (affixed to the outer pouch), and a reference thermocouple located externally in the centre location.

In this work, we will focus on the successful operation of the thermistor sensors in the cells' electrolytic environment, with full details of the instrumentation process to be detailed in an upcoming paper.

The findings from the analyses are discussed in the next section. The construction of the cells, and comprehensive analysis of their performance will be detailed in a second dedicated paper.

4. Results and discussion

This study aims to represent the chemical environment of a SIB, with electrolyte housed in glass vials. It is unlikely the sensors would be fully submerged within the liquid electrolyte continuously in a real SIB, so this

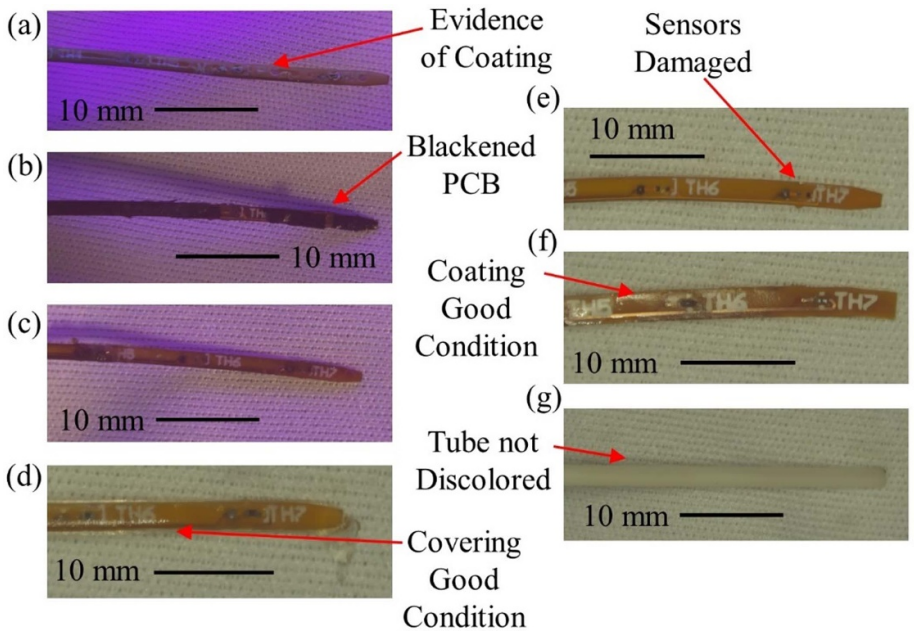

Figure 3. Photographs of PCBs post-submersion in electrolyte, (a)–(c) conformal coated PCBs shown under UV light to visualise tracer presence; (d)–(g) taken with standard lighting. Photographs show condition of PCBs with coatings as follows: (a) epoxy coating type (iii), (b) polyurethane coating type (ii), (c) acrylic coating type (i), (d) heat shrink tube covering, (e) PCB with no coating, (f) Parylene coated PCB and (g) reference thermocouple sensor.

is considered a worst-case scenario. However, in this work the temperature was kept constant (~25 °C), thus variation, which could exacerbate the ageing of the coating, was not studied.

4.1. Sensor data analysis

The data logging system was stopped after the 8-week period, and the vials removed from the block heater, figure S3. Visual inspection of the vials demonstrated the coating (iii) epoxy based, did not discolour the electrolyte, whereas the vials with other coating materials changed colour. This was checked at 6 weeks duration, figure S3(a), as well as after the experiment, (b), (c) and (d). Notably the liquid in the thermocouple sensor vials was also discoloured, although these sensors did not require any coating (ceramic tube were used to shroud the wires, described in previous work [23]). In this prior work, LIBs instrumented with these ceramic tube shrouded thermocouples demonstrated comparable performance to non-modified cells. Potentially these lithium systems are less sensitive to degradation through chemical contamination. It is noted, during fabrication, SIB components may need stricter controlled conditions compared to LIBs, for example, in general sodium-ion chemistries exhibit greater sensitivity to moisture (leading to faster degradation) [42].

The discoloration is likely to indicate the electrolyte is contaminated–quantified below via NMR experimentation. Naturally, during battery assembly, as the electrolyte is reactive to moisture, the processes are performed in dry rooms [43], else risk large capacity degradation among other issues and safety concerns [44, 45]. As the samples were stored in a typical laboratory environment, moisture could ingress around the vial lid or a reaction with the glass itself (electrolyte is typically stored in aluminium containers, in a dry glovebox). Moisture has previously been reported to cause discoloration, and perhaps indicate formation of HF [46–48]; however the electrolyte within all three of the epoxy based vials remained translucent throughout, similarly with three reference vials (filled with electrolyte for the 8 week period, but no sensors inserted–not shown in the figure).

The PCBs are shown removed from the vials in figure 3. There is visually observable damage to the polyurethane coated PCB (b), which has reacted with the electrolyte. From the three conformal coatings, shown figures 3(a)–(c), only the epoxy coating type (iii) has visible coating remaining after the study (purple tracer visible on image). The tube covering (d) was noted also to be in good condition.

The thermistor sensors have been proven to produce reliable and stable measurements during previous studies involving LIB instrumentation testing [49]. No cycling or change in temperature was actuated during the study, thus stable operation was expected at the constant temperature setpoint of 25 °C. The temperature and resistance data for the thermistor sensors are shown in figures 4(a) and (b), respectively, over a period of 60 d. Temperature data is plotted relative to the baseline set by the block heater (25 °C). The graphs show a

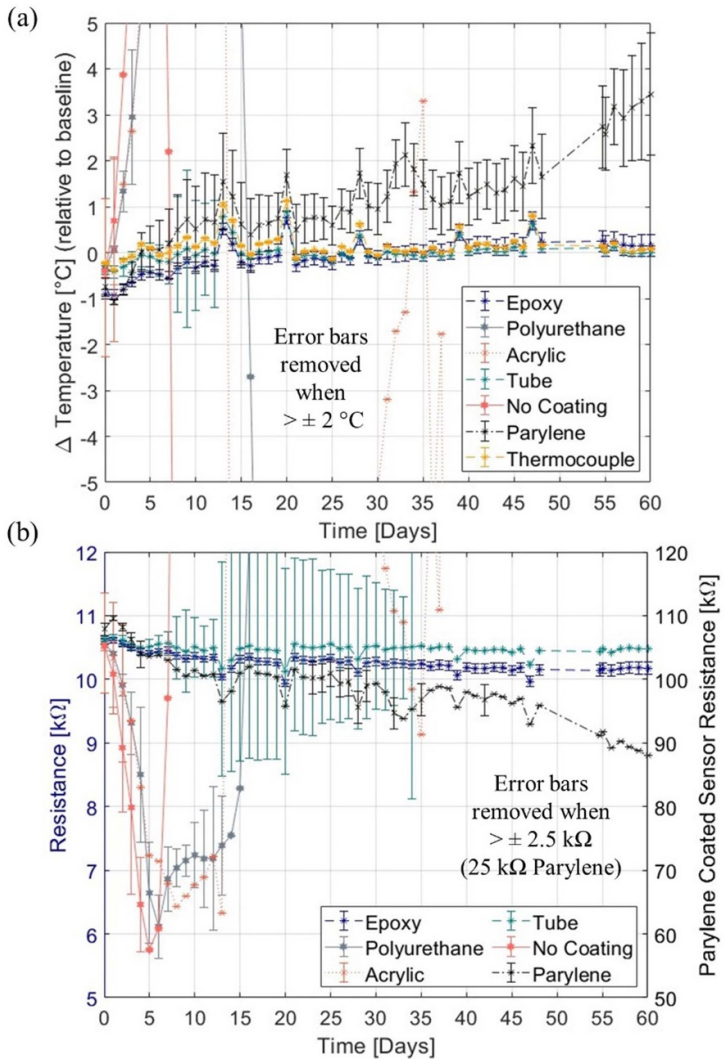

Figure 4. Data acquired from the sensors submerged in the electrolyte vials, (a) temperature data (thermistor sensors with thermocouple reference) and (b) resistance data (thermistor sensors only).

combined representation of all the sensors, with the median shown for each group (i.e. typically 6 sensors). The error bars indicate the standard deviation of each group; for readability, in plot (a) temperature error bars >2 °C length are removed and for (b) resistance error bars are removed for >2.5 kΩ length (for all sensors, accept the Parylene coated thermistors, which are set to a maximum of 25 kΩ). This is particularly noted for the tube covered sensors, where one pair failed (1 PCB), causing large error to be observed across the samples (error +3 °C); theses error bars were removed for improved readability.

Figure 4(a) demonstrates the sensors coated with coating type (iii) epoxy based are the only coating group resilient to the electrolyte. The acrylic based coating type (i) and polyurethane based (ii) begin to fail after only a period of 1.5 and 2 d, respectively, only slightly longer than the un-coated devices (1 d). Here, the failure is noted as a sharp change in temperature not observed with the reference thermocouple (>1 °C). The relative stability of the reference sensor demonstrates the unit is adequate for this experiment.

Maximum variation observed with thermocouple sensor was around 1 °C. The temperature data shown was taken from as a median of a 2-hour period, outside of laboratory hours–selected to give a representative reading, unaffected by environmental temperature fluctuations. The Parylene coated sensors initially perform well (all temperature readings within ±0.5 °C), however after ∼4 d, the readings from one pair of sensors starts to increase (indicating a decrease in resistance). This trend continues, where after 60 d, the median reading is ∼3 °C hotter than the reference thermocouple. With this extreme exposure to the electrolyte, the Parylene coating proved resilient for ∼4 d, which thereby would likely indicate suitability for a significant period of cell instrumentation, considering the chemical conditions within a cell. Potentially this could be related to the thickness of the coating, i.e. a thicker coating (or re-applying) could extend the life of

the sensor, however, any reaction with the electrolyte (analysed via NMR data below) would still indicate an unsuitable coating.

4.2. NMR data analysis

Multinuclear NMR spectroscopy was performed on electrolyte samples recovered from each vial to analyse the chemical composition of the electrolyte solution post-PCB-submersion experiment. Firstly, proton NMRs (^{1}H NMR) were used to investigate the potential presence of HF and water; secondly fluorine NMRs (^{19}F NMR)—to investigate the degradation products of the $NaPF_6$ salt contained in the electrolyte (i.e. the F_6 component) and identify/confirm the presence of HF; finally, phosphorous NMRs (^{31}P NMR) were performed to verify any further degradation product arising from the salt. A summary of the collected data is shown in figure 5.

The ^{1}H NMR analyses were used not only to identify decomposition of the coatings, but also to verify the vials were securely sealed, and the ingress of moisture from the environment was not the cause of electrolyte degradation. Figures 5(a)–(d) shows enlarged views of the ^{1}H NMR spectra from: fresh electrolyte (taken from the original container), non-coated, acrylic, Parylene and epoxy coated sensor vials. Notable regions of interest are shown in (a)–(d), used to investigate and highlight the presence of ethylene carbonate (EC) solvent, diethyl carbonate (DEC), general degradation and HF, respectively.

The assembly process of the vials and sensors was performed identically for all coatings–all vials were closed and sealed during one laboratory session, with the sensors all dried over the same period together in a drying chamber. Notable regions in figures 5(a) and (b) are attributable to the presence of ethylene carbonate (EC) and diethyl carbonate (DEC solvents), respectively, but do not demonstrate features related to decomposition. Figure 5(c) instead exhibits signals detected as a result of solvent decomposition. Notably all the coatings show a level of degradation compared to the fresh sample, although the epoxy-based coating indicates very limited degradation. The presence of HF in the spectrum in figure 5(d)–typically visible in the range of $>$10 ppm shift [50]–is visible for non-coated, acrylic and Parylene coated sensors and likely attributed to the reactivity of the sensor coating with the electrolyte.

No HF traces are detected in the fresh electrolyte and the epoxy sample, suggesting an improved chemical resistance of the epoxy coating toward the electrolyte. Also notable for the failed coated/non-coated sensors was the degradation observed in the electrolyte around the region of 4.3 ppm shift, potentially indicating presence of water [51]. Across both these regions, the epoxy coated sensor does not indicate presence of additional components compared to a fresh electrolyte sample.

To verify the formation of HF, and other potential salt deriving decomposition products, ^{19}F NMR was conducted–figure 5(e) presents an overview of the ^{19}F NMR spectra, with regions enlarged to highlight the possible presence of HF (f) and a range of other impurities identified via peaks in the $\sim$80 ppm range, (g). Similarly, the electrolyte contained in the vial with the epoxy coated sensor provides a spectrum with least contamination visible from additional species.

There are notable variation in the spectra for the samples taken from vials containing the non-coated, acrylic and Parylene coated sensors–figure 5(f) highlights the region typically indicating the presence of HF [50, 52]. The Parylene coating proved resilient against the electrolyte for the longest period compared to the other failed film coating methods (section 4.1), however the spectrum here indicates the failure has led to a reaction with the electrolyte. Although a thicker coating may extend resilience, the reaction (and therefore degradation in electrolyte) is not acceptable.

There are further impurities visible in these spectra in the region of $\sim$70–90 ppm, figure 5(g). Interestingly, the P-F rich decomposition products, previously attributed to hydrolysis products such as $PO_2F_2^{2-}$ or POF_3^- [53], as well as HF [50, 52] are detected for all samples except for the fresh electrolyte and the epoxy sample, further confirming its chemical stability against the electrolyte. For the purpose of this work, the NMR results are used to indicate the degradation of the sensor coatings and therefore impact on electrolyte purity, without focus on identifying precise chemical changes.

The ^{31}P NMR spectra figure 5(h) shows the distinctive pattern for $NaPF_6$ in the 140 ppm region [53]. Additional signals are visible in the -5 to -30 ppm region (i), which are commonly attributed to compounds forming during electrolyte degradation [50, 52–54].

The three NMR analyses performed qualitatively detects a series of compounds responsible of the observed electrolyte degradation as a result of its reactivity with the different coatings and potentially the sensors underneath. The results highlight that for the majority of the coatings, degradation occurs upon prolonged exposure to the electrolyte, while the epoxy coated sensors presents a reduced reactivity showing no presence of HF or other P-F rich compounds, with NMR profiles resembling the ones of the fresh electrolyte. We propose, these NMR spectra indicate no degradation of the epoxy coating during the experiment, i.e. any reaction between the coating and electrolyte would be result in an altered profile,

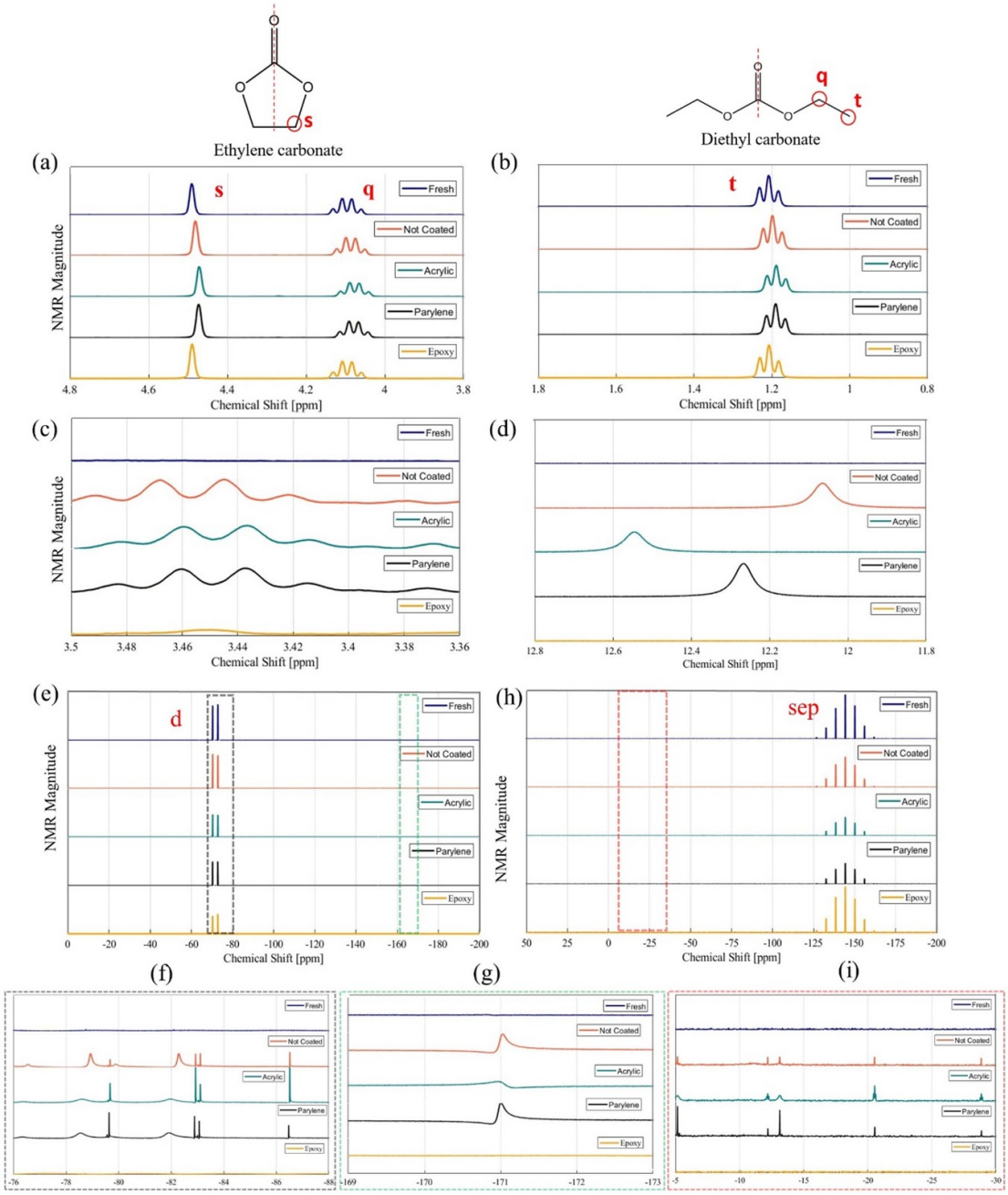

Figure 5. Analysis of NMR spectroscopy including representative data of electrolyte recovered from vials after chemical compatibility test. (a) to (d) ^{1}H NMR data, (e) to (g) ^{19}F NMR data and (h) & (i) ^{31}P NMR data. Regions to indicate presence of: (a) water and ethylene carbonate (EC); (b) diethyl carbonate (DEC); (c) decomposition of solvents components (visible in all coatings except epoxy-based); (d) HF presence. (e) Overview of ^{19}F NMR spectra and (f) further evidence of possible HF formation, not visible on fresh or epoxy-based coating spectra; (g) peaks indicating decomposition products in non-coated, acrylic and Parylene coatings. Note in (a) is from $NaPF_6$., (h) overview of ^{31}P NMR spectra; (i) enlarged view of P-F rich decomposition products visible in spectrum from samples taken from non-coated, acrylic and Parylene vials. Note, Note, *s* = singlet, *d* = doublet, *q* = quartet, *t* = triplet, sep = septet signals.

regardless of the magnitude of the degradation. Importantly, for successful cell instrumentation, the coating must be resilient throughout the lifetime of the cell (i.e. it cannot be re-applied).

4.3. Coin cell sensor experimentation

Samples of the coated sensor arrays were taken to test performance at coin-cell level; small sections of coated flexible PCB were cut from the end of freshly coated arrays. Prior to cell assembly, the arrays were dried for 24 h at 50 °C. A coin cell in full cell configuration (CR 2032) was built for each sample, composing of hard carbon anode, Prussian white cathode and two cellulose fiber-based separators (Dreamweaver Gold™), exact composition of the electrodes cannot be stated due to business confidentiality. Each cell contained a sensor

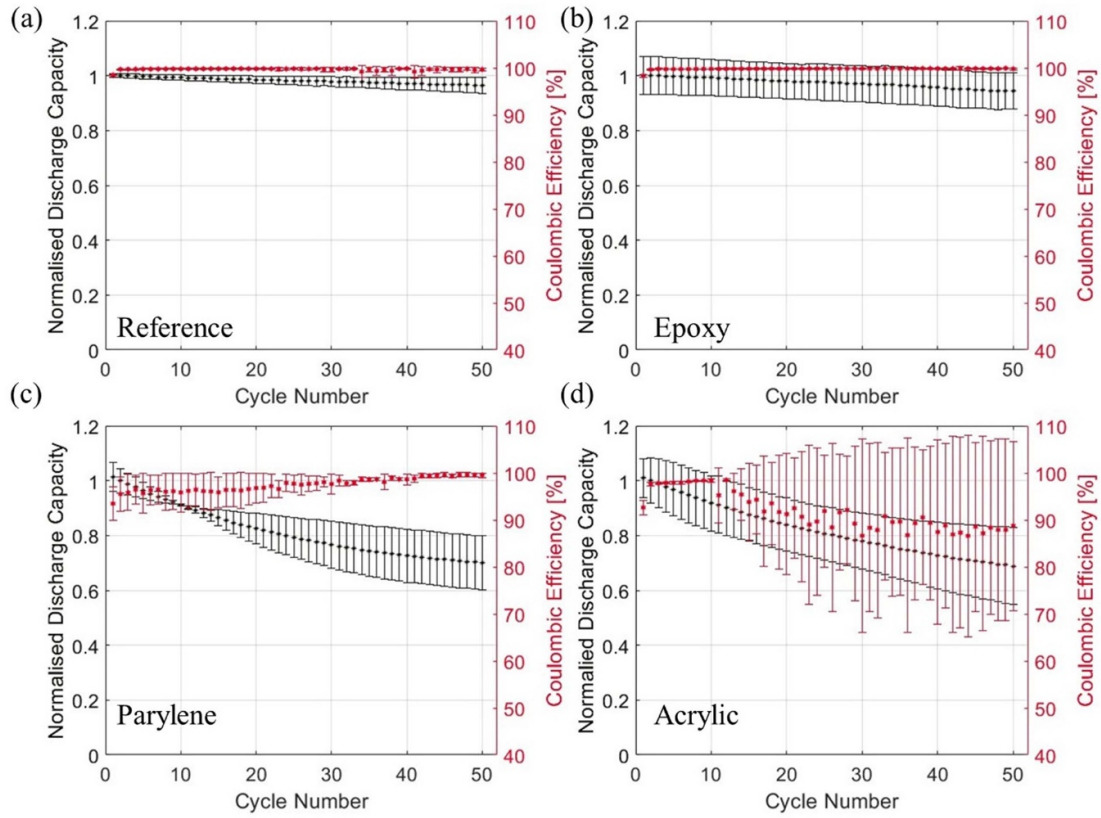

Figure 6. Plots showing average discharge capacity and CE over cycle number from coin cells with and without the coated sensors: (a) reference, (b) epoxy coated, (c) Parylene and (d) acrylic coated. Average data was constructed from 3 cells for each sample.

internally placed on top of the separator facing the anode, as shown in figure 2. Cells were then filled with 120 μl of fresh electrolyte and were tested under galvanostatic cycling test (constant current regime) between 1.3–3.8 V for 50 cycles at 25 °C. Initially, cells went through five formation cycles at 0.1 C charge/discharge and subsequently charged/discharged at 0.2 C with constant voltage charging applied until the supply current dropped below 0.05 C The discharge capacity and CE were examined for each cycle for comparison against a reference cell (constructed identically, but with no sensor). Figure 6 summarises the data recorded from the coin cells; for comparison normalised discharge capacity is presented.

Compared to the reference cell in figure 6(a), the CE data in figure 6(d), demonstrates the rapid degradation of the cell containing the acrylic coated sensor sample. The large deviation reflects the different order of magnitude of degradation for different electrolyte samples, which was also reflected in the error bars reported in figure 4 during the DAQ test from the sensors submerged in the electrolyte vials, however it is worth mentioning that in this case sensors are not recording any data. Notably, the cell containing the Parylene coated sample, degrades quickly (reduced to around 70% on average of its initial capacity after 50 cycles). However, in the case of the epoxy containing cells (figure 6(b)) improved performance was observed with a cycling stability resembling the one of the cells cycled without sensor. The purpose of these flexible PCBs is to study temperature gradients across larger cells, where for initial trials, the PCB will not be placed in the active region. Therefore, the focus of this work is to determine if the coatings degrade cell performance during their operation. Furthermore, the differences observed in the extent of capacity reduction are the consequence of the coating's compatibility with the electrolyte. As illustrated in the NMR observations, both acrylic and Parylene based coatings resulted to be unstable in the electrolyte thus exhibiting poor cycling performance and CE relative to the reference cells. The data supports the epoxy coating has minimal effect on cell performance and demonstrates reliable operation throughout the testing regime in agreement with the NMR analysis. Degradation in terms of capacity retention after 50 cycles was calculated as approximately 3.7%, 5.7%, 31% and 31.8%, for the reference, epoxy, Parylene and acrylic coated sensors, respectively.

4.4. Pouch cell sensor experimentation

Instrumentation of an A7 pouch cell forms the final step in verifying the sensor coating layer, where here a thermistor sensor array is successfully embedded within a cell, without degrading cell performance. We focus

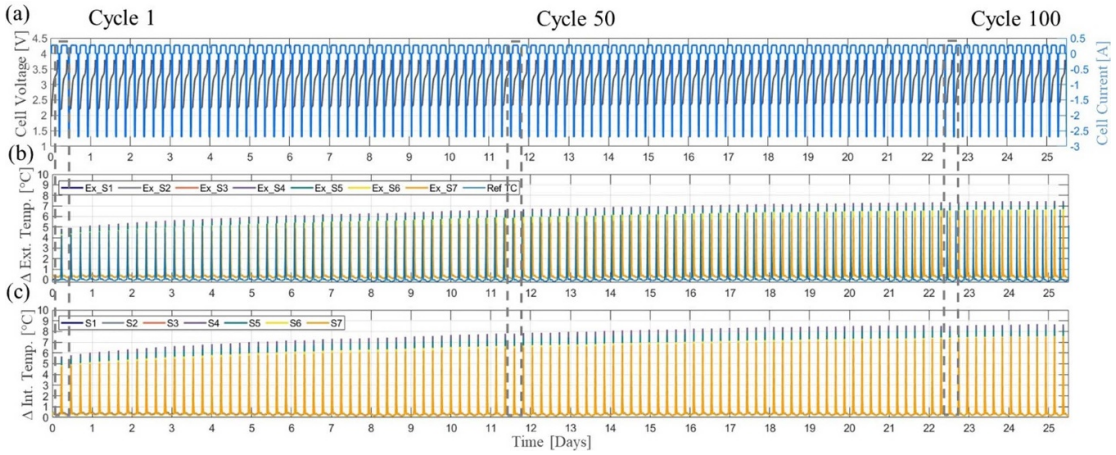

Figure 7. Cell cycling data and temperature data extracted from a representative A7 sized pouch cell, (a) current and voltage data, (b) external thermistor and thermocouple data and (c) internal thermistor data. Temperature data relative to initial temperature measurements (chamber temperature 25 °C).

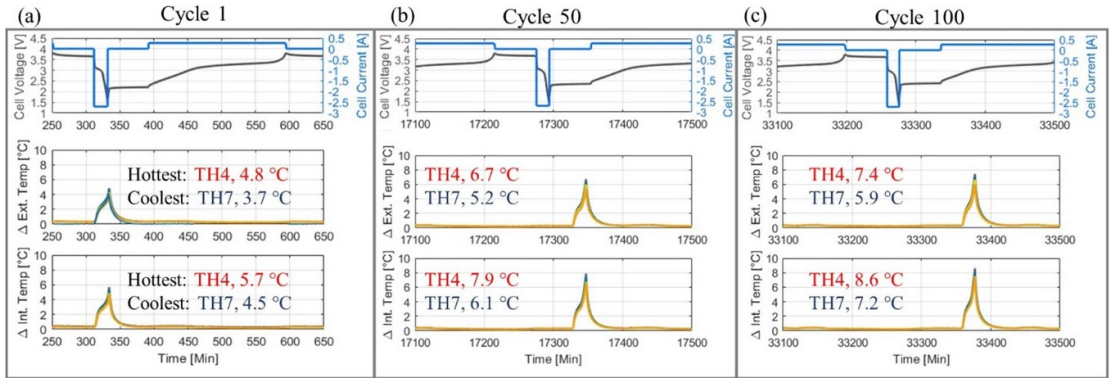

Figure 8. Enlarged plots showing data recorded at cycle 1, cycle 50, and cycle 100, in (a)–(c), respectively. Hottest peak temperatures (external top and internal lower plots) annotated, with coolest corresponding point recorded at the time the hottest temperature was observed.

on demonstrating sensor operation over 100 cycles, and ensuring cell capacity is consistent with an unmodified cell.

A sensor substrate, containing seven thermistor sensors was placed on top of the electrode stack (figure 2(b)), coated with the epoxy-based coating. In this work, we focus on the operation of the sensors and the cell. Data were logged at 5 Hz, shown here in a time-series plot, figure 7, demonstrating the reliable operation over a 25 day period (>100 cycles). The cell, typically termed a 1 Ah cell–named Cell 3 here- was cycled at a charge rate of 0.2 C and discharge rate of 2 C, with 1 h rest periods between each charge and discharge event. Voltage and current data are displayed in (a). Thermistor data are shown in (b) and (c), external and internal sensors, respectively. A reference thermocouple is located in the external centre of the cell (nearest thermistor location is TH4).

Enlarged plots of the first cycle, cycle 50 and cycle 100 are shown in figures 8(a)–(c), respectively. Sensor colours used to denote their location is shown in the legends in figures 7(b) and (c). The peak temperature (observed during the 2 C discharge stage) is shown for both the internal external thermistor arrays. Further analysis of cell temperature gradients will be published in an upcoming article; here we also note the coolest temperature locations recorded (at the time where the peak temperature was observed). It is noted for each cycle, the hottest temperatures are recorded in the centre of the cell (TH4), and the coolest sensors are those at the edge of the cell furthest away from the tabs (TH7).

The modified cells demonstrate lower initial capacity compared to the reference cells (a loss of ∼9%)–potentially this is due to the installation of the sensor, and will be investigated in further work. The cell data reported here (figure 7) exhibits higher degradation (12.4% after 100 cycles). The sensor data demonstrates excellent performance throughout, therefore suggesting there is no significant degradation of the coating, which therefore we propose the sensor does not affect cell performance.

Table 4. Summary of results by coating type after either >8 weeks submerged in electrolyte or cell instrumentation.

Coating type	PCB notes post-submersion	NMR findings	Cell notes
(iii) Epoxy based	All sensors operational (match performance of thermocouple). Only type to not discolour electrolyte inside vial.	Comparable data to fresh electrolyte. No HF detected.	**Coin:** Good performance, within typical expectations for this type of cell. **Pouch:** Comparable performance to reference-unmodified cell. Valid sensor data demonstrated after 100 cycles.
(ii) Polyurethane based	PCB badly corroded. Failure within 2 d.	Sample strongly degraded.	—
(i) Acrylic based.	Results from 5 sensors obtained. Coating visibility removed; sensors fail. Failure within 2 d.	HF detected. Numerous other compounds detected indicating failure.	**Coin:** Poor performing cell, discharge capacity drops rapidly with cycling. **Pouch**: Not tested–due to poor performance in coin cell.
(iv) Polyolefin tube.	1 pair of sensors observed drift in response. 2 remaining tube covered PCBs were resilient.	—	—
None.	Quickest failure observed (around 1 d).	—	**Coin:** Cell condition too poor to cycle. **Pouch**: Not tested–due to poor submersion test results.
(v) Parylene.	100 kΩ thermistors used. Out of 2 PCBs under test, 1 failed with considerable temperature drift.	HF detected. Other compounds present, indicating decomposition.	**Coin:** Stable performance during cycling. **Pouch:** Not tested–due to early failures during submersion testing.
Reference Thermocouple.	Stable output. Note some variation due to heater control.	—	—

4.5. Results summary

Our experimental findings support the use of epoxy-based sensor coating as a suitable material for protecting flexible PCBs for cell insertion without impacting cell performance. Performance-wise, the sensors reported excellent temperature sensing capability (reliable and accurate measurements compared to reference thermocouple) during electrolyte submersion. In terms of cell performance, these coated sensors had least impact on cell performance, and our NMR studies demonstrated the coating did not degrade nor contaminate the electrolyte solution. Table 4 summarises the findings from each coating type.

Epoxy has been previously reported in the case of LIB fibre optic instrumentation [55] and for general installation of components within smart cells [8]. For the first time, our results demonstrate the suitability of this epoxy based with comprehensive chemical analyses, whereas these previous works have used epoxy-based materials without verifying potential longer term degradation.

5. Further work

This work comprehensively analysed the condition of both the PCBs and electrolyte after the coated sensors had been submerged in the electrolyte containing vials for an 8-week period. To continue this work, we propose extending the study period for a longer duration. Lengthening the submersion period would verify if the cases of partial sensor failure were assembly error, or degradation in the chemical solution; i.e. failures were observed for one Parylene coated PCB and one tube coated PCB, where sensors began to degrade after a period of less than 1 week–the remaining PCBs of each coating type continued stable operation throughout the study period.

It is proposed the vials are heated to a higher temperature in further experiments, e.g. 35 or 45 °C, which is consistent with the typical temperatures reached by a cell during cycling [7]. This could potentially accelerate degradation, and while using the same heating equipment, alleviate fluctuations due to ambient temperature variation (i.e. here block heater device was only capable of heating, not chilling if ambient temperature rises above setpoint). Verifying operation at lower temperatures (e.g. 5 or 15 °C) would also be of interest, to ensure correct operation if the cell was to be used in cooler conditions (e.g. for experiments

involving detection of plating). Additional reference ambient temperature sensors could be placed on or around the heater block to understand variation in and around the unit.

In this work, three additional types of coating (acrylic, epoxy and polyurethane) were trialled beyond those prior art. These coatings were selected to offer a range of material composites, although future work could extend this investigation to refine material selection. Our selection criteria focused on manufacturing scalability, which we propose the three selected coatings meet–this will be further investigated through development of a spray coating rig. This application method would be suitable for scalability compared to the brush-on method described here; potentially offering improved uniformity, reduced application time and consistency between batches. Noting, in this study, the creating a thin coating (100 μm or lower) was not prioritised–here we investigated any coating-electrolyte reaction regardless of coating thickness. Any visible degradation via UV inspection (figure 3) or NMR analyses (figure 5) led to the coating being classified as unsuitable–potentially a thicker coating could extend sensor life, although this would be unacceptable due to reaction with the electrolyte affecting cell performance. To further verify the coatings will not eventually degrade over a longer period, measurements of film thickness across the surface of the substrate would allow uniformity and, if measured pre- and post- experiment, surface degradation, to be assessed.

The coatings were only trialled with flexible PCBs which were only populated with thermistor sensors. In future work, we propose trials including additional sensor types as well as sensor assemblies. For example: current, pressure or gas sensors; electronic circuitry/components and other smart cell control systems. Preferred conformal coatings were identified given this SIB electrolyte, and this study has demonstrated a successful methodology to test sensor coating compatibility (without needing live cells). Due to the different chemical compositions of other SIB and LIB electrolytes, it must be recommended this methodology is repeated to assess compatibility on a per-electrolyte basis. We propose extending our trials to verify compatibility with a range of common LIB electrolytes. A reduced study-size and targeted approach could be employed, potentially reducing the study time (i.e. failure often demonstrated within 5 d).

6. Conclusions

Here we have successfully identified an off-the-shelf, affordable and scalable coating suitable for protecting sensors to be instrumented within SIBs. Prior to this work, studies typically reported Parylene coatings were favoured to protect and prepare sensors (e.g. thermocouples [26]). Here, we have demonstrated a brush-on epoxy-based coating provides excellent chemical protection with minimal impact on cell performance.

Three new types of coatings were applied to the populated PCBs, based on acrylic, polyurethane and epoxy materials, which were not submersed in vials of SIB electrolyte for a period of 8 weeks. Temperature data were used to assess the feasibility of the coating protecting the sensor components within the harsh electrolytic environment. Consistent data were observed from the epoxy coated sensors, remaining within ± 1 °C of the reference thermocouples. The acrylic and polyurethane coated sensors all failed within <2 d period. Two Parylene coated PCBs were tested, one producing unreliable data within 4 d, whilst the other remained consistent with the reference. We surmise the harsh environment created by using pure electrolyte (and continuous complete submersion) simulates a worst-case scenario. Similarly, one of the PCBs covered with polyolefin tube (previously used to instrument live cells [6]) began to report erroneous measurements within 10 d. These failures could be due to damage during the sensor/vial assembly process, supporting the need for a coating that is both physically and chemically robust.

NMR analyses (^{1}H NMR, ^{19}F NMR and ^{31}P NMR) of samples were performed to demonstrate both possible contamination of the electrolyte (by comparison to fresh samples), as well as indicating degradation or reaction of the coating. No additional components were identified on spectra from epoxy-coated compared to those from fresh samples. Numerous additional species were found on the spectra for the acrylic, Parylene and polyurethane data. The highest magnitude signals were attributed to the degradation of the electrolyte and presence of HF and H_2O.

Observations of coin cells (containing sensor samples), namely discharge capacity and CE, were used to determine potential electrochemical reactivity of the coated sensors. The cell with epoxy sensor was the only type to offer comparable degradation after 50 cycles, relative to the reference cell ($<5\%$ capacity loss). Cell experimentation was extended to include A7 pouch cells ($\sim$1 Ah capacity), with functioning sensors recording data. Three modified (sensor instrumented) cells were tested, compared to two reference cells. Higher capacity was observed for the unmodified cells, although we propose this is due to the manual instrumentation process, which we will further develop in our upcoming work. The capacity fade was comparable to the unmodified variants (12.4% after 100 cycles for the modified cell). Temperature data was recorded throughout the period of 100 cycles ($\sim$25 d), 0.2 C charge, 2 C discharge, where excellent data (no spurious data points, no drift) were recorded. This compares favourably to the uncoated data in our

preliminary electrolyte vial experiments, and is consistent with the good performance observed from the epoxy coated sensors in the vials.

The epoxy-based coating is preferred for future SIB instrumentation, particularly for pouch cell experimentation, where minimising sensor thickness and avoiding non-uniform layouts are essential. Further work also includes extending the sensor type under-test as well as trialling protection of other electronic components.

Data availability statement

The data cannot be made publicly available upon publication because they contain commercially sensitive information. The data that support the findings of this study are available upon reasonable request from the authors.

Acknowledgments

Funding was received from the European Union's Horizon 2020 research and innovation program under Grant No. 883753 (Sodium-Ion and Sodium Metal Batteries for efficient and sustainable next-generation energy storage—SIMBA project).

Conflict of interest

The authors declare that they have no known competing financial interests or personal relationships that could have appeared to influence the work reported in this paper.

ORCID iDs

Timothy A Vincent https://orcid.org/0000-0002-3520-6610
Faduma M Maddar https://orcid.org/0000-0003-2160-4834
Erdogan Guk https://orcid.org/0000-0002-6198-2795
Jonathan E H Sansom https://orcid.org/0000-0003-1668-5609
Begum Gulsoy https://orcid.org/0000-0001-8169-5243
Mark Copley https://orcid.org/0000-0002-6435-8680
Ivana Hasa https://orcid.org/0000-0002-9099-5464
James Marco https://orcid.org/0000-0001-6827-0830

References

[1] Hirsh H S, Li Y, Tan D H S, Zhang M, Zhao E and Meng Y S 2020 Sodium-ion batteries paving the way for grid energy storage *Adv. Energy Mater.* **10** 2001274
[2] Hounjet L J 2022 Comparing lithium- and sodium-ion batteries for their applicability within energy storage systems *Energy Storage* **4** e309
[3] Hasa I *et al* 2021 Challenges of today for Na-based batteries of the future: from materials to cell metrics *J. Power Sources* **482** 228872
[4] Díaz-González F, Chillón-Antón C, Llonch-Masachs M, Galceran-Arellano S, Rull-Duran J, Bergas-Jané J and Bullich-Massagué E 2022 A hybrid energy storage solution based on supercapacitors and batteries for the grid integration of utility scale photovoltaic plants *J. Energy Storage* **51** 104446
[5] Hasa I, Barker J, Elia G and Passerini S 2023 Sodium-ion batteries: history, development, and overview on market and application *Ref. Modul. Chem. Mol. Sci. Chem. Eng.* (https://doi.org/10.1016/B978-0-323-96022-9.00061-X)
[6] Vincent T A, Hasa I, Gulsoy B, Sansom J E H and Marco J 2022 Battery cell temperature sensing towards smart sodium-ion cells for energy storage applications *2022 IEEE 16th Int. Conf. on Compatibility, Power Electronics, and Power Engineering (CPE-POWERENG)* pp 1–6
[7] Vincent T A, Gulsoy B, Sansom J E H and Marco J 2022 In-situ instrumentation of cells and power line communication data acquisition towards smart cell development *J. Energy Storage* **50** 104218
[8] Wei Z, Zhao J, He H, Ding G, Cui H and Liu L 2021 Future smart battery and management: advanced sensing from external to embedded multi-dimensional measurement *J. Power Sources* **489** 229462
[9] Turner L 2022 Battery tech advances *Renew: Technology for a Sustainable Future* (Renew/Alternative Technology Association) pp 66–72
[10] Fortier A, Tsao M, Williard N, Xing Y and Pecht M 2017 Preliminary study on integration of fiber optic bragg grating sensors in Li-ion batteries and *in situ* strain and temperature monitoring of battery cells *Energies* **10** 838
[11] Epp A and Sauer D U 2022 Multiperspective optimization of cell and module dimensioning for different lithium-ion cell formats on geometric and generic assumptions *Energy Technol.* **10** 2100874
[12] Sattarzadeh S, Roy T and Dey S 2021 Real-time estimation of 2D temperature distribution in lithium-ion pouch cells *IEEE Trans. Transp. Electr.* **7** 2249–59
[13] Bridgewater G, Capener M J, Brandon J, Lain M J, Copley M and Kendrick E 2021 A comparison of lithium-ion cell performance across three different cell formats *Batteries* **7** 38

[14] Mayyas A, Steward D and Mann M 2019 The case for recycling: overview and challenges in the material supply chain for automotive li-ion batteries *Sustain. Mater. Technol.* **19** e00087
[15] World Economic Forum (WEF) 2019 *A Vision for A Sustainable Battery Value Chain in 2030* (available at: https://www.weforum.org/publications/a-vision-for-a-sustainable-battery-value-chain-in-2030/)
[16] Chayambuka K, Mulder G, Danilov D L and Notten P H L 2020 From Li-ion batteries toward Na-ion chemistries: challenges and opportunities *Adv. Energy Mater.* **10** 2001310
[17] Gao Y, Jiang J, Zhang C, Zhang W, Ma Z and Jiang Y 2017 Lithium-ion battery aging mechanisms and life model under different charging stresses *J. Power Sources* **356** 103–14
[18] Liu T *et al* 2019 Exploring competitive features of stationary sodium ion batteries for electrochemical energy storage *Energy Environ. Sci.* **12** 1512–33
[19] Martins L S, Guimarães L F, Botelho Junior A B, Tenório J A S and Espinosa D C R 2021 Electric car battery: an overview on global demand, recycling and future approaches towards sustainability *J. Environ. Manage.* **295** 113091
[20] Mohr M, Peters J F, Baumann M and Weil M 2020 Toward a cell-chemistry specific life cycle assessment of lithium-ion battery recycling processes *J. Ind. Ecol.* **24** 1310–22
[21] Sun Y *et al* 2020 Development and challenge of advanced nonaqueous sodium ion batteries *EnergyChem* **2** 100031
[22] Curnick O J, Sansom J E H, Harper J, Tsiamtsouri M, Bhagat R and Greenwood D 2019 Rapid state-of-health (SoH) determination and second-life grading of aged automotive battery modules via electrochemical impedance spectroscopy (EIS) *ECS Meeting Abstr.* **MA2019-02** 53
[23] Gulsoy B, Vincent T A, Sansom J E H and Marco J 2022 In-situ temperature monitoring of a lithium-ion battery using an embedded thermocouple for smart battery applications *J. Energy Storage* **54** 105260
[24] Niri M F, Bui T M N, Dinh T Q, Hosseinzadeh E, Yu T F and Marco J 2020 Remaining energy estimation for lithium-ion batteries via Gaussian mixture and Markov models for future load prediction *J. Energy Storage* **28** 101271
[25] Bruen T and Marco J 2016 Modelling and experimental evaluation of parallel connected lithium ion cells for an electric vehicle battery system *J. Power Sources* **310** 91–101
[26] Zhang G, Cao L, Ge S, Wang C-Y, Shaffer C E and Rahn C D 2014 In situ measurement of radial temperature distributions in cylindrical Li-ion cells *J. Electrochem. Soc.* **161** A1499–507
[27] Amietszajew T *et al* 2019 Hybrid thermo-electrochemical *in situ* instrumentation for lithium-ion energy storage *Batter. Supercaps* **2** 934–40
[28] Yu Y, Vergori E, Worwood D, Tripathy Y, Guo Y, Somá A, Greenwood D and Marco J 2021 Distributed thermal monitoring of lithium ion batteries with optical fibre sensors *J. Energy Storage* **39** 102560
[29] Novais S *et al* 2016 Internal and external temperature monitoring of a Li-ion battery with fiber bragg grating sensors *Sensors* **16** 1394
[30] Meyer J, Nedjalkov A, Doering A, Angelmahr M, Schade Jan Meyer W and Schade W 2015 Fiber optical sensors for enhanced battery safety *Proc. SPIE* **9480** 190–201
[31] Ghannoum A, Iyer K, Nieva P and Khajepour A 2017 Fiber optic monitoring of lithium-ion batteries: a novel tool to understand the lithiation of batteries *Proc. IEEE Sensors* (https://doi.org/10.1109/ICSENS.2016.7808695)
[32] Li H, Wei F, Li Y, Yu M, Zhang Y, Liu L and Liu Z 2021 Optical fiber sensor based on upconversion nanoparticles for internal temperature monitoring of Li-ion batteries *J. Mater. Chem.* C **9** 14757–65
[33] Lee C Y, Lee S-J, Hung Y-M, Hsieh C-T, Chang Y-M, Huang Y-T and Lin J-T 2017 Integrated microsensor for real-time microscopic monitoring of local temperature, voltage and current inside lithium ion battery *Sens. Actuators* A **253** 59–68
[34] Zhu S, Han J, An H-Y, Pan T-S, Wei Y-M, Song W-L, Chen H-S and Fang D 2020 A novel embedded method for *in-situ* measuring internal multi-point temperatures of lithium ion batteries *J. Power Sources* **456** 227981
[35] Vincent T A and Marco J 2020 Development of smart battery cells through sensor instrumentation and in-vehicle power line communication *2020 IEEE Int. Symp. on Power Line Communications and Its Applications, ISPLC 2020* (https://doi.org/10.1109/ISPLC48789.2020.9115411)
[36] Stephenson A, Willsey M, McBride J, Newman S, Nguyen B, Takahashi C, Strauss K and Ceze L 2020 PurpleDrop: a digital microfluidics-based platform for hybrid molecular-electronics applications *IEEE Micro* **40** 76–86
[37] Chong H, Majerus S J A, Bogie K M and Zorman C A 2020 Non-hermetic packaging of biomedical microsystems from a materials perspective: a review *Med. Devices Sens.* **3** e10082
[38] Cai T, Valecha P, Tran V, Engle B, Stefanopoulou A and Siegel J 2021 Detection of Li-ion battery failure and venting with carbon dioxide sensors *eTransportation* **7** 100100
[39] Kalaga K, Rodrigues M T F and Abraham D P 2018 In situ lithiated reference electrode: four electrode design for in-operando impedance spectroscopy *J. Vis. Exp.* **139** e57375
[40] Kogel-Hollacher M, Breier M, Schröder D and Schulze J 2017 The next level—controlled conformal coating processes *Opt. Photon.* **12** 18–21
[41] Murata Manufacturing Co. Ltd 2021 NCP03WF104F05RL|NTC for temperature sensor *Murata Temperature Sensors* (available at: www.murata.com/en-eu/products/productdetail?partno=NCP03WF104F05RL)
[42] Zhang R, Yang S, Li H, Zhai T and Li H 2022 Air sensitivity of electrode materials in Li/Na ion batteries: issues and strategies *InfoMat* **4** e12305
[43] Dai F and Cai M 2022 Best practices in lithium battery cell preparation and evaluation *Commun. Mater.* **3** 1–6
[44] Han J G, Jeong M-Y, Kim K, Park C, Sung C H, Bak D W, Kim K H, Jeong K-M and Choi N-S 2020 An electrolyte additive capable of scavenging HF and PF5 enables fast charging of lithium-ion batteries in LiPF6-based electrolytes *J. Power Sources* **446** 227366
[45] Yaghoobnejad Asl H, Sharma S and Manthiram A 2020 The critical effect of water content in the electrolyte on the reversible electrochemical performance of Zn–VPO4F cells *J. Mater. Chem.* A **8** 8262–7
[46] Aguesse F, Manalastas W, Buannic L, Lopez Del Amo J M, Singh G, Llordés A and Kilner J 2017 Investigating the dendritic growth during full cell cycling of garnet electrolyte in direct contact with Li metal *ACS Appl. Mater. Interfaces* **9** 3808–16
[47] Wang C *et al* 2019 Overlooked electrolyte destabilization by manganese (II) in lithium-ion batteries *Nat. Commun.* **10** 1–9
[48] Yang D, Li X, Wu N and Tian W 2016 Effect of moisture content on the electrochemical performance of LiNi1/3Co1/3Mn1/3O2/graphite battery *Electrochim. Acta* **188** 611–8
[49] Vincent T A, Gulsoy B, Sansom J E H and Marco J 2021 A smart cell monitoring system based on power line communication—optimization of instrumentation and acquisition for smart battery management *IEEE Access* **9** 161773–93
[50] Rinkel B L D, Hall D S, Temprano I and Grey C P 2020 Electrolyte oxidation pathways in lithium-ion batteries *J. Am. Chem. Soc.* **142** 15058–74

[51] Tułodziecki M, Leverick G M, Amanchukwu C V, Katayama Y, Kwabi D G, Bardé F, Hammond P T and Shao-Horn Y 2017 The role of iodide in the formation of lithium hydroxide in lithium–oxygen batteries *Energy Environ. Sci.* **10** 1828–42
[52] Wiemers-Meyer S, Winter M and Nowak S 2016 Mechanistic insights into lithium ion battery electrolyte degradation—a quantitative NMR study *Phys. Chem. Chem. Phys.* **18** 26595–601
[53] Ould D M C, Menkin S, O'Keefe C A, Coowar F, Barker J, Grey C P and Wright D S 2021 New route to battery grade $NaPF_6$ for Na-ion batteries: expanding the accessible concentration *Angew. Chem., Int. Ed.* **60** 24882–7
[54] Ravdel B, Abraham K M, Gitzendanner R, DiCarlo J, Lucht B and Campion C 2003 Thermal stability of lithium-ion battery electrolytes *J. Power Sources* **119–121** 805–10
[55] Yu Y, Vincent T, Sansom J, Greenwood D and Marco J 2022 Distributed internal thermal monitoring of lithium ion batteries with fibre sensors *J. Energy Storage* **50** 104291